Smart Grid and Renewable Energy, 2024, 15, 34-48
https://www.scirp.org/journal/sgre
ISSN Online: 2151-4844
ISSN Print: 2151-481X

Online Capacitor Voltage Transformer Measurement Error State Evaluation Method Based on In-Phase Relationship and Abnormal Point Detection

Yongqi Liu[1,2], Wei Shi[1*], Jiusong Hu[1,2], Yantao Zhao[2], Pang Wang[2]

[1]College of Railway Transportation, Hunan University of Technology, Zhuzhou, China
[2]Wasion Group Co., Ltd., Changsha, China
Email: *shiwei@hut.edu.cn

How to cite this paper: Liu, Y.Q., Shi, W., Hu, J.S., Zhao, Y.T. and Wang, P. (2024) Online Capacitor Voltage Transformer Measurement Error State Evaluation Method Based on In-Phase Relationship and Abnormal Point Detection. *Smart Grid and Renewable Energy*, **15**, 34-48.
https://doi.org/10.4236/sgre.2024.151003

Received: December 18, 2023
Accepted: January 23, 2024
Published: January 26, 2024

Abstract

The assessment of the measurement error status of online Capacitor Voltage Transformers (CVT) within the power grid is of profound significance to the equitable trade of electric energy and the secure operation of the power grid. This paper advances an online CVT error state evaluation method, anchored in the in-phase relationship and outlier detection. Initially, this method leverages the in-phase relationship to obviate the influence of primary side fluctuations in the grid on assessment accuracy. Subsequently, Principal Component Analysis (PCA) is employed to meticulously disentangle the error change information inherent in the CVT from the measured values and to compute statistics that delineate the error state. Finally, the Local Outlier Factor (LOF) is deployed to discern outliers in the statistics, with thresholds serving to appraise the CVT error state. Experimental results incontrovertibly demonstrate the efficacy of this method, showcasing its prowess in effecting online tracking of CVT error changes and conducting error state assessments. The discernible enhancements in reliability, accuracy, and sensitivity are manifest, with the assessment accuracy reaching an exemplary 0.01%.

Keywords

Capacitor Voltage Transformer, Measurement Error, Online Monitoring, Principal Component Analysis, Local Outlier Factor

1. Introduction

The Capacitor Voltage Transformer (CVT) finds extensive application in the

measurement and control of high-voltage power grids, along with energy measurement in systems of 110 kV and above [1] [2]. Its commendable insulation properties and economic viability contribute to its widespread usage. Nonetheless, its intricate structure results in a failure rate five times higher than that of the electromagnetic voltage transformer (PT) [3], posing a significant challenge to the equitable trade and secure operation of electrical energy.

Currently, the prevalent method for addressing such faults involves offline verification during power outages in the grid. However, this approach, requiring periodic power interruptions, suffers from low verification efficiency and inherent delays. Consequently, there is an imperative to investigate online evaluation methods applicable under non-power outage conditions [4].

Literature [5] [6] presents diagnostic methods grounded in physical or mathematical models of the component, but these are constrained by a singular usage environment and lack versatility due to the intricate nature of influencing factors. Signal processing-based detection methods proposed in existing literature fail to eliminate primary side power grid fluctuations [7] [8] [9], risking misjudgments or omissions during prolonged monitoring. Another proposed evaluation method relies on high-dimensional random matrices, addressing error changes on the order of 0.1% but exhibiting reduced accuracy for changes on the order of 0.01% [10]. State assessment methods based on principal component analysis (PCA) [11] and independent component analysis (ICA) [12] can identify error changes on the order of 0.1%, yet they falter in the face of significant three-phase voltage imbalances observed in real-world environments.

In summary, existing methods exhibit the following drawbacks:

- Long-term quantitative online monitoring of CVT error status remains unattained.
- The impact of CVT primary side voltage fluctuations on error state assessment persists due to changes in grid load.
- Insufficient sensitivity to CVT error changes results in low accuracy in error state assessment.

This manuscript introduces a method for online evaluation of CVT error states, anchored in the principles of in-phase correlation and outlier detection. The chronological data in the time series serve to segregate the metrics that depict the error states, discerning alterations in the CVT by assessing whether the metrics deviate significantly from the norm. Ultimately, a threshold is applied to enable real-time surveillance of the CVT's error status. This approach adeptly mitigates voltage amplitude fluctuations, ensuring steadfast, precise, and perceptive online monitoring of the CVT error status, achieving an accuracy level of up to 0.01%.

2. Preliminaries

2.1. CVTs Measurement Principle

The Capacitor Voltage Transformer (CVT) stands as an instrument for measur-

ing grid voltage. It adeptly transforms the elevated voltage on the primary side into a diminished voltage on the secondary side, with its pivotal parameter being the conversion ratio, elegantly illustrated in **Figure 1**. Nevertheless, swayed by the prolonged operation of the Capacitor Voltage Transformer (CVT) and structural malfunctions, its factual transformation ratio undergoes a certain degree of alteration. Consequently, this leads to measurement errors in both the measurement and control processes. Errors are divided into ratio errors and phase errors according to different description objects. The errors in this article all refer to ratio errors. The magnitude of the ratio error can be delineated by Equation (1):

$$\varepsilon(t)=\frac{k_r u(t)-U(t)}{U(t)} \tag{1}$$

Whereas k_r denotes the nominal transformation ratio, $U(t)$ represents the amplitude of the primary (primary side input) voltage, and $u(t)$ symbolizes the amplitude of the secondary (measure side output) voltage at time *t*.

In accordance with the stipulations of the relevant standards, the permissible limits for measurement errors in CVTs of varying precision levels, operating at their rated voltages, are elucidated in **Table 1**. For the 0.2 precision level CVT, typically employed in commercial transactions, the ratio differential should not exceed ±0.2% [13] [14]. Should the calibration error of a CVT surpass the error threshold of its corresponding precision level, the CVT is deemed to be beyond tolerance and necessitates repair or replacement.

Each set of CVT-n consists of three different phase CVTs, The primary side of the CVTs interfaces directly with the expansive power grid. Subject to the load, the voltage experiences an unsettled state of fluctuation. Distinguishing whether these fluctuations stem from changes in CVT error poses a pivotal and challenging issue that demands resolution in the evaluation. The dual busbar configuration is extensively employed in high-voltage power grids, with its wiring topology illustrated in **Figure 2**.

W1 and **W2** denote the high-voltage buses linked to the extensive power grid, while the primary sides of all CVTs are connected to the busbars through switches. In the regular operation of the power grid, all switches are in a closed state. When the three-phase unbalance of the bus is not considered, capture the power frequency signal from the CVTs measurement and control coil, where the coil load is negligible, indicating that the primary voltage of the CVT aligns with the bus voltage at this juncture. However, the power grid outlet adheres to a three-phase structure, susceptible to three-phase voltage imbalances due to load variations. This difference is essential for assessment of metering errors and becomes difficult to detect, and becomes indiscernible. Hence, our focus shifts to the in-phase CVT to mitigate the impact of load fluctuations and enhance the precision of error assessment. For in-phase CVT, its secondary side voltage can be mathematically expressed as Equation (2):

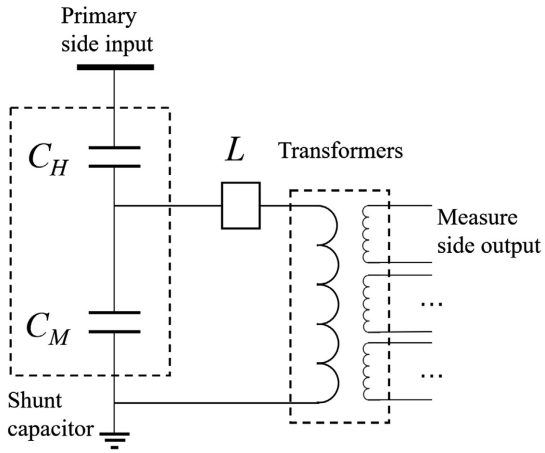

Figure 1. CVT structure schematic diagram.

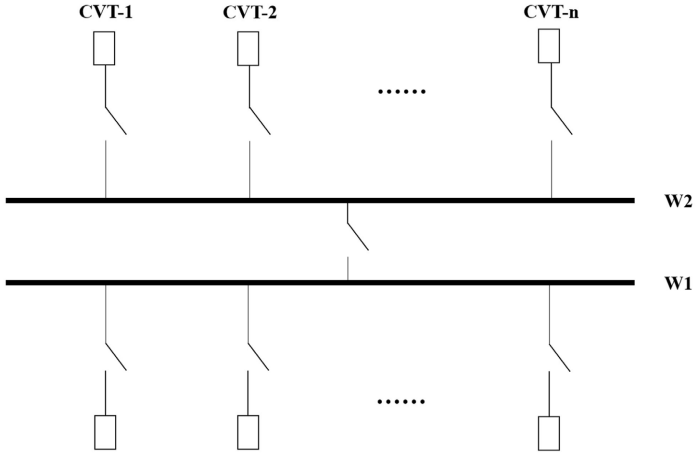

Figure 2. Schematic diagram of double busbar connection system.

Table 1. Accuracy level measurement error limits.

Accuracy level	Ratio Error Limit
0.1	0.1%
0.2	0.2%
0.5	0.5%

$$\begin{pmatrix} u_1(t) \\ u_2(t) \\ \vdots \\ u_n(t) \end{pmatrix} = \begin{pmatrix} \frac{1+\varepsilon_1}{k_r} & 0 & \cdots & 0 \\ 0 & \frac{1+\varepsilon_2}{k_r} & \cdots & 0 \\ \vdots & \vdots & \ddots & \vdots \\ 0 & 0 & \cdots & \frac{1+\varepsilon_n}{k_r} \end{pmatrix} \times \begin{pmatrix} U(t) \\ U(t) \\ \vdots \\ U(t) \end{pmatrix} \tag{2}$$

2.2. Algorithm Principle

Pursuant to Equation (2), the secondary side measurement of each CVT is

composed of a veritable value and a dynamic error, the latter fluctuating with the passage of time. Consequently, by scrutinizing this chronicle of time-oriented measurements, deviations indicative of anomalous error behavior in CVTs can be discerned. For recently installed or recently validated CVTs, a methodology for detecting measurement errors based on in-phase relationships is posited. This method employs Principal Component Analysis (PCA) to project measurement values into the residual space encapsulating errors [15] [16] [17]. Detection of error changes in CVTs is then accomplished by computing the Local Outlier Factor (LOF) [18]. The method delineates two distinct stages: initialization modeling and online monitoring, with the primary steps outlined as follows:

- **Initialization Modeling 1**

During the initiation modeling 1, the voltage amplitude $X_{01}^{m\times n}=\left[x_1,x_2,\cdots,x_n\right]$ of the secondary side output is amassed. Here, m and n denote the number of samples at the sampling point and the number of CVTs, respectively. Standardization of X_{01} is performed to achieve a mean of 0 and a variance of 1, as illustrated in Equation (3).

$$\bar{X}=\left(X-E\left(X\right)\right)D^{-1} \tag{3}$$

where $E\left(X\right)=\left[\mu_1,\mu_2,\cdots,\mu_n\right]$ is the mean vector of x_i and $D=diag\left[\sigma_1,\sigma_2,\cdots,\sigma_n\right]$ is the standard deviation matrix. Where $\sigma_i=\sqrt{E\left(x_i-\mu_i\right)^2}$ is the standard deviation of x_i.

Subsequently, the covariance matrix $R^{n\times n}$ of matrix $\bar{X}$ is computed and diagonalized, as depicted in Equation (4).

$$R=\frac{1}{m-1}\bar{X}^{\mathrm{T}}\bar{X}=PVP^{\mathrm{T}} \tag{4}$$

where, $P^{n\times n}$ is a unitary matrix, and $V=diag\left[\lambda_1,\lambda_2,\cdots,\lambda_n\right]$ is a diagonal matrix, and the eigenvalue λ_i satisfies $\lambda_1>\lambda_2>\cdots>\lambda_n$.

At present, the number of pivots is determined by the accumulated contribution rate percentage of the variance (CPV). The CPV method determines the number of pivot components by calculating the cumulative variance percentage of the first k eigenvalues, as expressed in Equation (5).

$$\mathrm{CPV}\left(k\right)=\frac{\sum_{j=1}^{k}\lambda_j}{\sum_{i=1}^{n}\lambda_i}\times 100\% \tag{5}$$

When using the CPV method to select the number of pivots, you need to manually select a standard CPV expected value. Under normal circumstances, this value can be set to 85%. Combining the resultant $P^{n\times n}$ from Equation (4), The first $k\,(k<n)$ linearly independent vectors of P, $P_K=\left[P_1,P_2,\cdots,P_k\right]$ form the pivot space, and the last $n-k$ linearly independent vectors of P, $P_e=\left[P_{k+1},P_{k+2},\cdots,P_n\right]$ form the residual space.

The CVT error can be articulated as the projection of measurement data in

the residual space. An abnormal alteration in the measurement error state of CVT is manifested by a discernible deviation in the projection of measurement data within the pivot subspace and residual subspace. The degree of this deviation is ascertained by establishing statistics for the assessment of the CVT measurement error state. Generally, the Q statistic is established in the residual subspace to gauge the extent of deviation in the non-principal components of the measurement data, detailed in Equation (6).

$$Q_i = \bar{X}_i^2 = \left\| p_{ei} P_e^{\mathrm{T}} \bar{X}^{\mathrm{T}} \right\| \tag{6}$$

where $Q_i^{m\times 1}$ is the Q statistic of ith CVT, $\bar{X}_i$ is ith column vector of $\bar{X}$, p_{ei} is the ith column vector of P_e.

- **Initialization Modeling 2**

In contrast to sampling points devoid of error changes, those with error changes represent outliers, distinctly reflected in a mutation in the CVT's Q statistic. To sensitively and precisely detect alterations in Q and enhance the accuracy of CVT status monitoring, this paper introduces the Local Outlier Factor (LOF) algorithm. Key parameters of the algorithm are defined as follows:

During the initiation modeling 2, the voltage amplitude $X_{02}^{m\times n} = [x_1, x_2, \cdots, x_n]$ of the secondary side output is amassed. Using the PCA model obtained in initialization modeling 1, calculate the Q of each CVT. For CVT-i, data point q is the Q statistic calculated from initialization modeling 1 at time t, the data point o is a point in the data set $O = Q_i \in R^{m\times 1}$. The Euclidean distance between data points q and o is expressed as $d(q,o)$. The Euclidean distance between all points in the data set O and the data point q is expressed as $d = [d_1, \cdots, d_k, \cdots, d_m]$, and satisfies $d_1 \geq d_2 \geq \cdots \geq d_m$. The k-distance $d_{k\text{-distance}}$ of data point q can be expressed as Equation (7).

$$d_{k\text{-distance}} = d_k \tag{7}$$

All points with $d(q,o) \leq d_{k\text{-distance}}$ in the data set O constitute the k-distance neighborhood $N_{k\text{-distance}}(q)$ of data point q. The k-distance reachable distance $d_{kr}(q,o)$ from data point q to data point o can be expressed as Equation (8).

$$d_{kr}(q,o) = \max\left\{ d(q,o), d_{k\text{-distance}} \right\} \tag{8}$$

For any integer k, if the distance between data point q and data point o is sufficiently small, the $d_{k\text{-distance}}$ of data point q is the $d_{kr}(o,q)$ between the two data points (for example: when $k = 6$, in **Figure 3**, the $d_{kr}(o,q_1)$ between o and q_1 is the $d_{6\text{-distance}}$ of o). If the distance between data point q and data point o is considerable, the $d_{kr}(o,q)$ between the two data points is the $d(q,o)$ between them. Euclidean distance (for example: the 6th order reachable distance between o and q_2 in **Figure 3** is the $d(o,q_2)$ between them).

The local reachability density $lrd(q)$ of the data point q is the reciprocal of the average $d_{kr}(q,o)$ amid all data points within its $N_{k\text{-distance}}(q)$ and data point q, as delineated in Equation (9). This local reachable density efficaciously mirrors the distribution of other data points proximate to q. The smaller the value, the higher the possibility that the data point is an outlier.

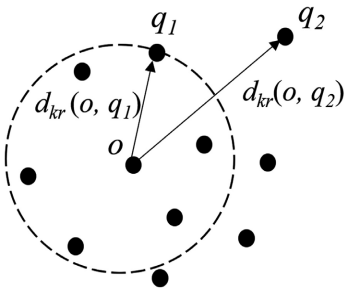

Figure 3. The 6th order reachable distance of data point o.

$$lrd(q)=\left(\frac{\sum_{o\in N_{k\text{-distance}}(q)} d_{kr}(q,o)}{N(q)}\right)^{-1} \tag{9}$$

where, $N(q)$ is the number of points in $N_{k\text{-distance}}(q)$.

The local outlier factor $lof(q)$ embodies the mean ratio of the $lrd(q)$ of data point q to the $lrd(o)$ of all data points within its $N_{k\text{-distance}}(q)$, elucidated in Equation (10).

$$lof(q)=\frac{\sum_{o\in N_{k\text{-distance}}(q)} \frac{lrd(o)}{lrd(q)}}{N(q)} \tag{10}$$

If data point q deviates from the known data population, resulting in a diminished $lrd(q)$, the local outlier factor $lof(q)$ surges disproportionately. Most data within a cluster exhibit an $lof(q)$ approximating 1, whereas data q with $lof(q)\gg 1$ signifies that $lrd(q)$ is inferior to the data within $N_{k\text{-distance}}(q)$, suggesting data q is an outlier. At this time, one of the monitored CVTs has an error change, which can be determined by the contribution degree, elucidated in Equation (11).

$$H_i^{-1}=\frac{lof_{ci}}{lof_i}\cdot\sum_{j=1}^{n}\frac{lof_j}{lof_{cj}} \tag{11}$$

where, lof_i and H_i represent the outlier factor and contribution of the ith CVT, and lof_{ci} represents the outlier factor of the limit error of the ith CVT at the corresponding accuracy level. lof_{ci} can be simulated by superimposing the limit error on the measured data of the CVT in X_{02}.

- **Online Monitoring**

Upon completion of the initialization, the secondary side voltage amplitude of the CVT is collected for online monitoring. Subsequently, Q_i and lof_i are calculated for each monitored CVT, and whether lof_i is an outlier is determined. When an outlier is detected, it indicates that there is an error change in the CVT being detected. After the CVT where the error changes occur is determined through the contribution degree, determining that the CVT is in an out-of-tolerance state if its lof_i surpasses the lof_{ci}.

3. Algorithm Flowchart

This paper introduces a CVT online error state evaluation method based on the in-phase relationship and outlier detection. Leveraging the minimal interference between in-phase CVTs, sampling points are projected into the residual space established through PCA during the initialization stage. The characteristic statistic Q, defining the CVT error state, is then calculated. Real-time detection of the Q statistic is achieved through the LOF algorithm. Ultimately, a threshold is employed to facilitate online quantitative monitoring of the CVT error state. The outlined steps are detailed below, and the algorithm flowchart is illustrated in Figure 4.

1) Initiate the gathering of secondary side output data from CVTs newly installed in the substation or those that have recently undergone periodic inspections. Formulate initialization datasets $X_0 = [X_{01}; X_{02}]$, and online monitoring dataset X_1.

2) Embark on the Initialization Modeling 1, wherein parameters μ and σ are meticulously computed. Standardize dataset X_{01}, followed by the implementation of PCA to derive the residual space parameter P_e.

3) Transition into the Initialization Modeling 2. Leverage parameters μ and σ to standardize dataset X_{02}. Compute the Q_i for each CVT, establish the $N_{k\text{-distance}}$, and ascertain the lof_{ci} under salient conditions.

4) Enter the online monitoring stage, executing real-time Q_i abnormal point detection on sampling points to ascertain alterations in the measurement error of the CVT. If such changes are detected, utilize the contribution degree to pinpoint the CVT undergoing an error change. Concurrently, assess whether the magnitude of this change surpasses the upper limit, thereby concluding the comprehensive evaluation of the error status of the sampling point.

4. Experiment and Result

In this section, we shall ascertain the efficacy of this methodology utilizing data derived from an authentic substation site. Initially, known error variations are incorporated into the collected dataset, thereby generating a myriad of test datasets. Subsequently, we evaluate the viability and precision of this approach for assessing the error states of CVTs. (The aforementioned verification process was executed using "MATLAB R2021a").

4.1. Data Description

The experimental data emanated from a substation located in northwest China, featuring a 330 kV double busbar structured CVT. Three groups, comprising 9 CVTs each, manufactured by Xi'an Xirong Power Capacitor Co., Ltd., model TYD330/−0.005H, with an accuracy level of 0.2, serve as the subjects. The initial error is presumed to be zero for experimental expediency, and the collection site is delineated in Figure 5.

This high-precision sampling apparatus operates at a frequency of once per

minute, meticulously sampling three sets of 9 CVTs over five consecutive days, aggregating 7200 sampling points per CVT. No conspicuous anomalies were observed during the entire sampling duration. Figure 6 depicts the primary side voltage amplitude restored from the collected voltage amplitude at the CVT secondary side output. The upper figure shows the three output voltage amplitudes of the first group of CVTs, and the lower figure shows the A-phase output voltage amplitudes of the three groups of CVTs. It can be seen from the curve that the same-phase relationship is more harmonious than the three-phase relationship.

4.2. Experimental Steps

1) Segregate the experimental dataset by extracting 2880 samples from the initial two days to formulate the initialization dataset $X_0 \in R^{2880\times9}$. The remaining samples are retained as online monitoring data sets $X_1 \in R^{4320\times9}$ without superimposed human errors.

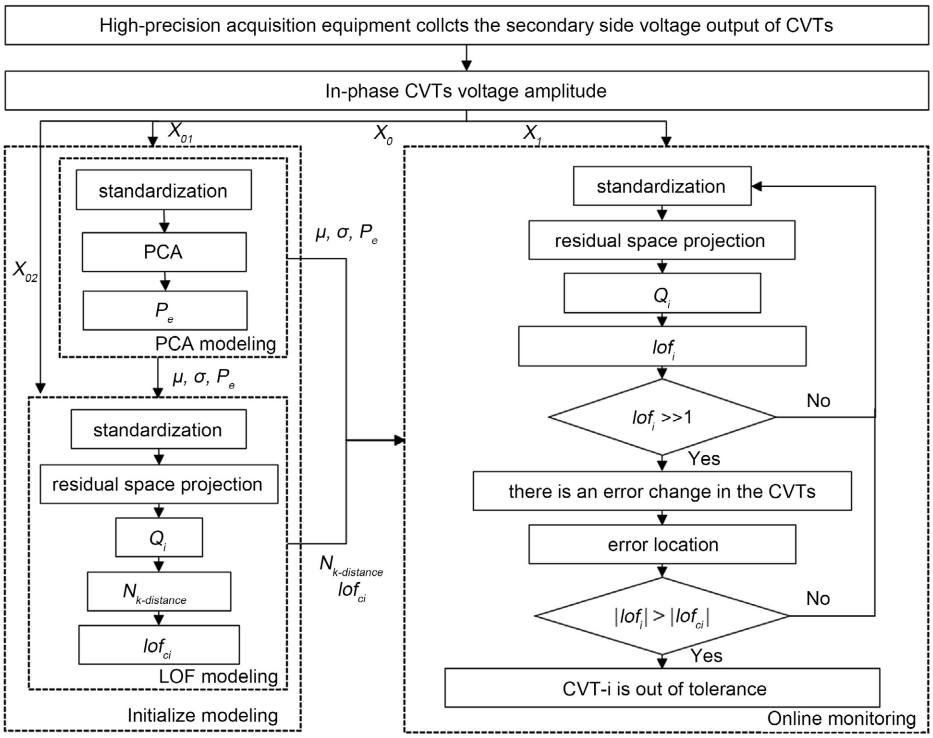

Figure 4. The flow chart of the online error state assessment method.

Figure 5. Substation data collection site.

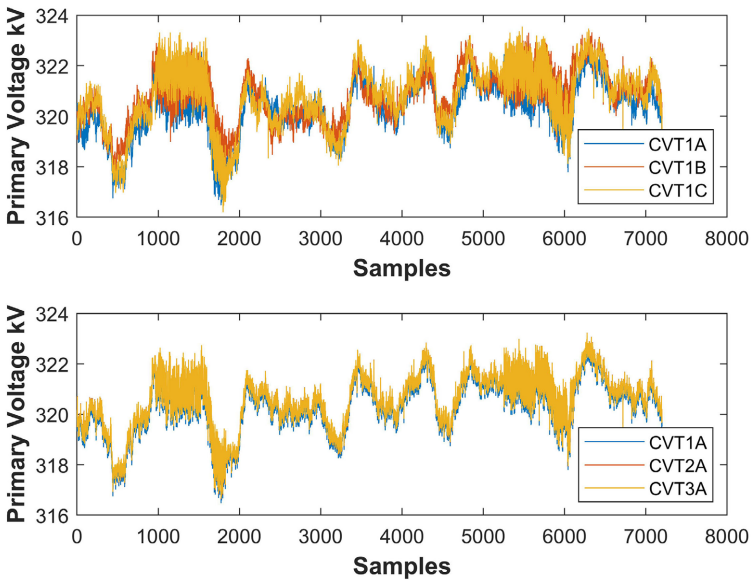

Figure 6. CVT primary side input voltage amplitude curve.

2) **Experiment 1:** Based on the first step, generate a substantial volume of online monitoring data incorporating known error changes. With reference to the CVT's accuracy level, generate 1000 error values per CVT, each with a resolution of 0.01% and adhering to a normal distribution, as depicted in **Figure 7**. Commencing from a randomly selected sampling point, superimpose these error values onto the dataset $X_1 \in R^{4320\times9}$ ($x' = x \times (1+\varepsilon)$, the errors in all experiments are superimposed and will not be explained again). Take these 90,000 experimental data sets as input, compare the evaluation outcomes and error setting values of this method, affirming the accuracy and sensitivity of the assessment method for CVT error states.

3) **Experiment 2:** Compare extant research methodologies to authenticate the precision and discernment of this approach in situations where the error state of an individual CVTs undergoes modification. Deriving from step 1, employ $X_1 \in R^{4320\times9}$ to formulate an experimental dataset $X_1' \in R^{4320\times9}$. This dataset entails superimposing errors onto CVT-1A multiple times, thereby orchestrating a transition in error status from the ordinary to an out-of-tolerance condition. The method for superimposing errors is elucidated in **Table 2**, wherein "sample point" designates the juncture at which error increments are overlaid. The remaining 8 CVTs retain unaltered data. Contrast the evaluation outcomes of literature [11] and literature [12] with the methodology propounded in this manuscript.

4.3. Results and Discussion

- **Experiment 1**

The subject of this experiment is a 0.2-level CVT. According to **Table 1**, it is discerned that the error range in its standard state is [−0.2%, 0.2%]. If the superimposed error value falls within this spectrum, it signifies that the CVT is in a

normal state; contrarily, it in an out-of-tolerance state. When the evaluation result is consistent with the predetermined CVT error state, it means that the evaluation is correct. Table 3 catalogues the number of correct instances and the accuracy rate of this method compared to the predefined values. As observed from the tabulation, over 9000 repetitions, the method articulated in this document was accurately assessed 8973 times, yielding a commendable accuracy rate of 99%. The experimental results affirm that this approach can efficaciously realize the evaluation of CVT error states under non-power outage conditions. Moreover, it remains impervious to the undulations in its primary measurement voltage. The method exhibits remarkable accuracy, even when faced with a plethora of errors reaching the critical value of 0.2% (−0.2%). This unequivocally substantiates the accuracy and sensitivity of this method in assessing error states, with a sensitivity reaching 0.01%.

Table 2. Experiment 2 error superposition method.

CVT Num	Sampling point	Error change	Current error value	State
CVT-1A	1 - 999	0.00%	0.00%	Normal
	1000	0.15%	0.15%	Normal
	2000	0.01%	0.16%	Normal
	3000	0.03%	0.19%	Normal
	3500	0.02%	0.21%	Out of tolerance
Other CVT	All	0.00%	0.00%	Normal

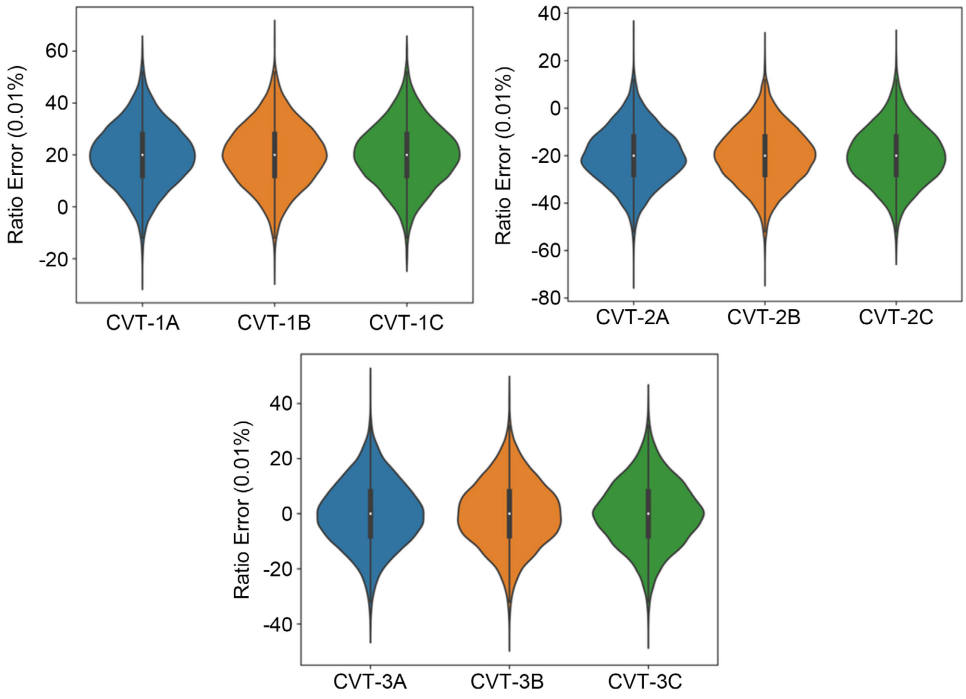

Figure 7. Error distribution of CVT experimental data superposition.

Table 3. The accuracy of the experimental results of Experiment 1.

CVT Num	Phase	Times	Correct rate
CVT-1	A	998	99.8%
	B	995	99.5%
	C	989	98.9%
CVT-2	A	1000	100.0%
	B	995	99.5%
	C	1000	100.0%
CVT-3	A	1000	100.0%
	B	997	99.7%
	C	999	99.9%
Total	\	8973	99.7%

- **Experiment 2**

Literature [11] and literature [12] are CVT error state evaluation methods proposed in the past two years. Judging from the experiments in the corresponding articles, the evaluation results are relatively outstanding. The experimental results of these two methods are shown in **Figure 8**. Whenever the evaluation result surpasses the predetermined threshold, it indicates a metamorphosis in CVT error. Beyond the 1000th sampling point, the CVT error undergoes a change, and the statistic Q (SPE) is anticipated to exceed the threshold and persist until the conclusion of the evaluation. This is overtly incongruent with the evaluation outcomes. Influenced by the three-phase imbalance in the power grid, these two methodologies falter in achieving theoretical efficacy concerning CVT error changes. They are inept at monitoring and tracking CVT error changes, rendering them inadequate for early warnings regarding out-of-tolerance states.

The evaluation results of this method are illustrated in **Figure 9**. At the 1000th, 2000th, and 3000th sampling points, the *lof* of the CVT undergoes a mutation, successfully monitoring the change in error, even when it is a mere 0.01%. At the 3000th sampling point, the CVT error registers at 0.19%, adhering to the error requirement for a 0.2-level CVT, aligning seamlessly with the evaluation results. By the 3500th sampling point, the CVT error escalates to 0.21%. At this juncture, the *lof* exceeds the threshold lof_c, prompting the algorithm to determine that the CVT has transitioned into an out-of-tolerance state. A comparative analysis between the evaluation curve and the error setting curve in **Figure 9** affirms the congruity in the *lof* change with the pre-established CVT error alteration. This further validates the appropriateness of the method delineated in this manuscript for online CVT error change monitoring and error state evaluation in network systems, bolstering accuracy and reliability.

As underscored in the review, this segment substantiates the feasibility and precision of this method for online CVT error state assessment through an extensive series of repeated experiments. Comparative analyses affirm that this

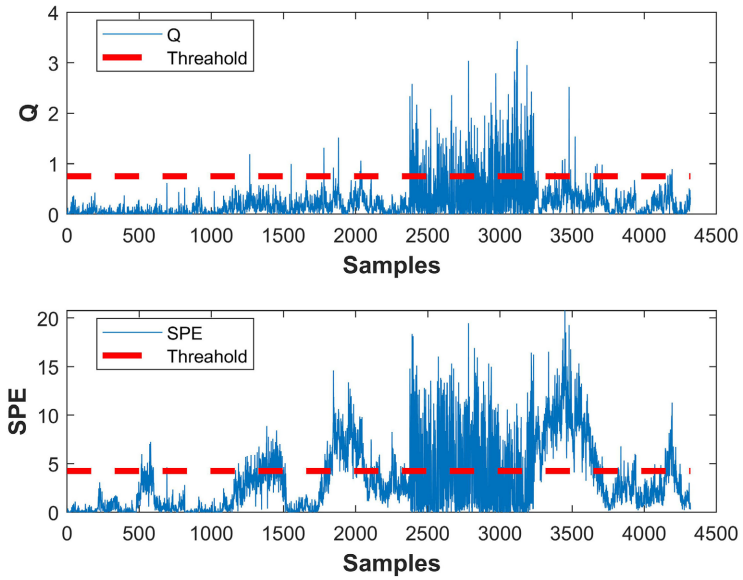

Figure 8. PCA and ICA method evaluation results.

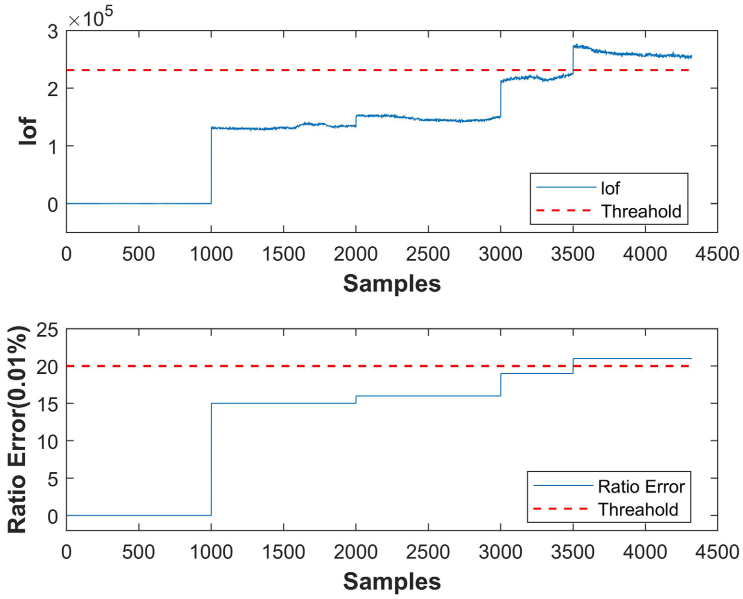

Figure 9. Evaluation results of this method.

method exhibits certain advantages over prevailing online evaluation methodologies in terms of accuracy, reliability, and sensitivity in tracking changes and assessing the status of errors.

5. Conclusions

This paper posits an online Capacitor Voltage Transformer (CVT) error state evaluation methodology predicated on the in-phase relationship and the identification of aberrant points. This approach adeptly achieves meticulous and discerning evaluation of the CVT error state under circumstances devoid of power outages, impervious to perturbations induced by the undulating grid voltage,

and attains a remarkable precision of 0.01%.

Influenced by the limitations inherent in the experimental conditions, the comprehensive validation of the efficacy of this method in prolonged field assessments remains incomplete. This constitutes the central concern of our forthcoming experimentation. Simultaneously, the exploration of methodologies for error status assessment in scenarios where the count of CVT groups is fewer than three demands further scrutiny, marking the pivotal axis of our subsequent endeavors and scholarly investigations.

Conflicts of Interest

The authors declare no conflicts of interest regarding the publication of this paper.

References

[1] Tolić, I., Miličević, K. and Malarić, R. (2019) The Impact of Current, Voltage and Phase Displacement Errors on the Cross-Border Energy Exchange. *Measurement*, **132**, 330-335. https://doi.org/10.1016/j.measurement.2018.09.014

[2] Bao, Z., Jiao, Y., Chen, M., Zhang, C. and Li, H. (2021) Online Anomaly Detection for the Measurement Error of HVPT in the Multi-Bus Structure. *Measurement*, **170**, Article 108722. https://doi.org/10.1016/j.measurement.2020.108722

[3] Zhang, F.Z., Liu, K., Huang, J.P. and Li, T. (2016) Research on Capacitor Voltage Transformer Error Online Monitoring System. *Electrical Measurement & Instrumentation*, **53**, 53-57.

[4] Meng, Z., Chen, Q., Li, H. and See, C.H. (2020) Internal Insulation Condition Identification for High-Voltage Capacitor Voltage Transformers Based on Possibilistic Fuzzy Clustering. *Review of Scientific Instruments*, **91**, Article 014705. https://doi.org/10.1063/1.5123438

[5] Chatterjee, P., Pal, A., Thorp, J.S., De La Ree Lopez, J. and Centeno, V.A. (2018) Error Reduction of Phasor Measurement Unit Data Considering Practical Constraints. *IET Generation, Transmission & Distribution*, **12**, 2332-2339. https://doi.org/10.1049/iet-gtd.2017.1359

[6] Wang, C., Centeno, V.A., Jones, K.D. and Yang, D. (2019) Transmission Lines Positive Sequence Parameters Estimation and Instrument Transformers Calibration Based on PMU Measurement Error Model. *IEEE Access*, **7**, 145104-145117. https://doi.org/10.1109/ACCESS.2019.2944818

[7] Xiong, X., He, N., Yu, J., Chen, X., Zi, M.R. and Hu, Z. (2010) Diagnosis of Abrupt-Changing Fault of Electronic Instrument Transformer in Digital Substation Based on Wavelet Transform. *Power System Technology*, **34**, 181-185.

[8] Dolce, S., Fiorucci, E., Bucci, G., D'Innocenzo, F., Ciancetta, F. and Di Pasquale, A. (2017) Test Instrument for the Automatic Compliance Check of Cast Resin Insulated Windings for Power Transformers. *Measurement*, **100**, 50-61. https://doi.org/10.1016/j.measurement.2016.12.039

[9] Azirani, M.A., Ariannik, M., Werle, P. and Akbari, A. (2021) Optimal Frequency Selection for Detection of Partial Discharges in Power Transformers Using the UHF Measurement Technique. *Measurement*, **172**, Article 108895. https://doi.org/10.1016/j.measurement.2020.108895

[10] Zhao, P., Ma, K.Q., Li, H.B., Zhou, F. and Chen, Q. (2022) Online Error Evaluation

Method of Instrument Voltage Transformers Considering Primary Voltage Fluctuations. *High Voltage Engineering*, No. 3, 48.

[11] Zhang, Z., Chen, Q., Hu, C., Li, H. and Chen, M. (2018) Evaluating the Metering Error of Electronic Transformers Online Based on VN-MWPCA. *Measurement*, **130**, 1-7. https://doi.org/10.1016/j.measurement.2018.07.083

[12] Zhang, C.J., Li, H.B. and Chen, Q. (2019) Detection of the Ratio Error Drift in CVT Considering AVC. *Measurement*, **138**, 425-432. https://doi.org/10.1016/j.measurement.2019.02.052

[13] IEC 61869-3: 2011 (2011) Instrument Transformers—Part 3: Additional Requirements for Inductive Voltage Transformers. https://webstore.iec.ch/publication/6051

[14] General Administration of Quality Supervision (2007) JJG 1021-2007 Verification Regulation of Instrument Transformers in Power System (Bejing, China), Inspection and Quarantine of the People's Republic of China.

[15] Zhang, M., Zhan, Y.M. and He, S.F. (2017) Power Quality Data Compression Based on Iterative PCA Algorithm in Smart Distribution Systems. *Smart Grid and Renewable Energy*, **8**, 366-378. https://doi.org/10.4236/sgre.2017.812024

[16] Zhu, Z., Ye, W.Z. and Kuang, H.J. (2021) Convergence Analysis of a Kind of Deterministic Discrete-Time PCA Algorithm. *Advances in Pure Mathematics*, **11**, 408-426. https://doi.org/10.4236/apm.2021.115028

[17] Salih, M.E., Zhang, X.M. and Ding, M.Y. (2022) Kernel PCA Based Non-Local Means Method for Speckle Reduction in Medical Ultrasound Images. *Open Access Library Journal*, **9**, e8618. https://doi.org/10.4236/oalib.1108618

[18] Long, K., Wu, Y.H. and Gui, Y.F. (2018) Anomaly Detection of Store Cash Register Data Based on Improved LOF Algorithm. *Applied Mathematics*, **9**, 719-729. https://doi.org/10.4236/am.2018.96049